

NUCLEAR DYNAMICS AT THE GEOMETRY OF VANISHING FLOW IN HEAVY-ION COLLISIONS

*M. Kaur*¹

Department of Physics, Panjab University, Chandigarh, India

We study the time evolution and mass dependence of various quantities (such as average and maximum central density, collision dynamics, participant spectator matter, and average and maximum temperature) at the geometry of vanishing flow (GVF) throughout the mass range between 80 and 262 units. We find that the reaction time at 100 MeV/nucleon of the geometry of vanishing flow is smaller for lighter nuclei compared to heavier ones. All the quantities can be parameterized by a power law dependence. The maximal values of corresponding quantities are also shifted accordingly.

Изучается эволюция во времени и зависимость от массы различных величин (таких как средняя и максимальная центральные плотности, динамика столкновения, материя-спектатор и средняя и максимальная температуры) в геометрии исчезающего потока в интервале масс от 80 до 262 единиц. Исследование показывает, что время реакции в геометрии исчезающего потока при 100 МэВ/нуклон меньше для более легких ядер по сравнению с тяжелыми. Все величины можно параметризовать степенной зависимостью. Максимальные значения соответствующих величин сдвигаются в соответствии с таким же принципом.

PACS: 24.10.Pa; 25.70.Pq

INTRODUCTION

The heavy-ion reactions at intermediate energies have been used extensively over the last three decades to investigate the hot and dense nuclear matter that also shed light on nuclear matter equation of state (EOS) as well as on in-medium nucleon–nucleon (nn) cross section. Among various phenomena, collective transverse in-plane flow [1–3] has been found to be one of the most sensitive observables. Lot of experimental as well as theoretical efforts have been made to study the transverse in-plane flow [4]. The variation in the flow as a function of beam energy reflects the competition between the attractive (due to mean field) and repulsive interactions (due to nucleon–nucleon collisions). At a particular energy, the net transverse in-plane flow vanishes, since the strengths of these two interactions counterbalance each other. This energy is termed as energy of vanishing flow (EVF) [2]. The EVF has been found to be sensitive to the mass of the colliding system [2, 5–7]. A power law mass dependence (αA^τ) of EVF has also been reported in the literature.

¹E-mail: mandeep.pu@gmail.com

The colliding geometry, on the other hand, also plays an important role in determining the flow as well as its disappearance. As one moves away from the perfectly central collisions, the transverse flow increases, reaching a maximum at semicentral collisions, then decreases and finally switches to negative domain due to lack of binary nucleon–nucleon scattering. The value of impact parameter where collective flow vanishes (crosses zero) is termed as geometry of vanishing flow (GVF) [7]. This study revealed the sensitivity of the system size of GVF to the nucleon–nucleon cross section as well as to momentum-dependent interactions.

In this report, we aim to look for the complete analysis of the dynamics at GVF throughout the mass range between 80 and 262 units. The present study is carried out within the framework of isospin-dependent molecular dynamics (IQMD) model [8,9], which is discussed below.

1. THE MODEL

In IQMD model, baryons are represented by Gaussian-shaped density distributions

$$f_i(\mathbf{r}, \mathbf{p}, t) = \frac{1}{\pi^2 \hbar^2} \exp\left(-[\mathbf{r} - \mathbf{r}_i(t)]^2 \frac{1}{2L}\right) \exp\left(-[\mathbf{p} - \mathbf{p}_i(t)]^2 \frac{2L}{\hbar^2}\right). \quad (1)$$

These hadrons propagate using the Hamilton equations of motion:

$$\frac{d\mathbf{r}_i}{dt} = \frac{d\langle H \rangle}{d\mathbf{p}_i}, \quad \frac{d\mathbf{p}_i}{dt} = -\frac{d\langle H \rangle}{d\mathbf{r}_i}, \quad (2)$$

with

$$\langle H \rangle = \langle T \rangle + \langle V \rangle = \sum_i \frac{p_i^2}{2m_i} + \sum_i \sum_{j>i} \int f_i(\mathbf{r}, \mathbf{p}, t) V^{ij}(\mathbf{r}', \mathbf{r}) f_j(\mathbf{r}', \mathbf{p}', t) d\mathbf{r} d\mathbf{r}' d\mathbf{p} d\mathbf{p}'. \quad (3)$$

The baryon potential V^{ij} , in the above relation, reads as

$$\begin{aligned} V^{ij}(\mathbf{r}' - \mathbf{r}) &= V_{\text{Skyrme}}^{ij} + V_{\text{Yukawa}}^{ij} + V_{\text{Coul}}^{ij} + V_{\text{sym}}^{ij} = \\ &= \left[t_1 \delta(\mathbf{r}' - \mathbf{r}) + t_2 \delta(\mathbf{r}' - \mathbf{r}) \rho^{\gamma-1} \left(\frac{\mathbf{r}' + \mathbf{r}}{2} \right) \right] + t_3 \frac{\exp(-|\mathbf{r}' - \mathbf{r}|/\mu)}{(|\mathbf{r}' - \mathbf{r}|/\mu)} + \frac{Z_i Z_j e^2}{|\mathbf{r}' - \mathbf{r}|} + \\ &\quad + t_4 \frac{1}{\rho_0} T_{3i} T_{3j} \delta(\mathbf{r}_i' - \mathbf{r}_j). \end{aligned} \quad (4)$$

Here $t_4 = 4C$ with $C = 32$ MeV and Z_i and Z_j denote the charges of the i th and j th baryon, and T_{3i} and T_{3j} are their respective T_3 components (i.e., $1/2$ for protons and $-1/2$ for neutrons). The parameters μ and t_1, \dots, t_4 are adjusted to the real part of the nucleonic optical potential. For the density dependence of the nucleon optical potential, standard Skyrme-type parametrization is employed.

2. RESULTS AND DISCUSSIONS

The «directed transverse momentum $\langle p_x^{\text{dir}} \rangle$ » used in the calculations reads as [10]

$$\langle p_x^{\text{dir}} \rangle = \frac{1}{A} \sum_{i=1}^A \text{sign}\{y(i)\} p_x(i), \quad (5)$$

where $y(i)$ and $p_x(i)$ are, respectively, the rapidity and momentum of the i th particle. The rapidity is defined as

$$y(i) = \frac{1}{2} \ln \frac{\mathbf{E}(i) + \mathbf{p}_z(i)}{\mathbf{E}(i) - \mathbf{p}_z(i)}, \quad (6)$$

where $\mathbf{E}(i)$ and $\mathbf{p}_z(i)$ are, respectively, the energy and longitudinal momentum of the i th particle. The value of the impact parameter at which flow disappears is termed as GVF, as we have discussed in Introduction.

For the present study, we simulated the reactions of $^{40}\text{Ca} + ^{40}\text{Ca}$, $^{58}\text{Ni} + ^{58}\text{Ni}$, $^{93}\text{Nb} + ^{93}\text{Nb}$, $^{118}\text{Sn} + ^{118}\text{Sn}$ and $^{131}\text{Xe} + ^{131}\text{Xe}$ at their respective geometry of vanishing flow (GVF) at an incident energy of 100 MeV/nucleon. The geometry of vanishing flow for these systems reads as 0.5, 0.6, 0.7, 0.7 and 0.8 [11]. In the following, we shall first study the time evolution and then present the mass dependence of different quantities.

First of all, we shall present results of nuclear density which is defined as

$$\rho(\mathbf{r}, t) = \frac{1}{A_P + A_T} \sum_{i=1}^{A_P + A_T} \frac{1}{(2\pi L)^{3/2}} \exp \left[\frac{-(\mathbf{r} - \mathbf{r}_i(t))^2}{2L} \right]. \quad (7)$$

Here A_T and A_P stand, respectively, for the mass of the target and projectile. In actual calculations, we take a sphere of radius 2 fm around the centre of mass and compute the density at each time step during the reaction using the above equation. Naturally, one can either extract an average density $\langle \rho^{\text{avg}} \rangle$ over the whole sphere or a maximal value of the density $\langle \rho^{\text{max}} \rangle$ reached anywhere in the sphere.

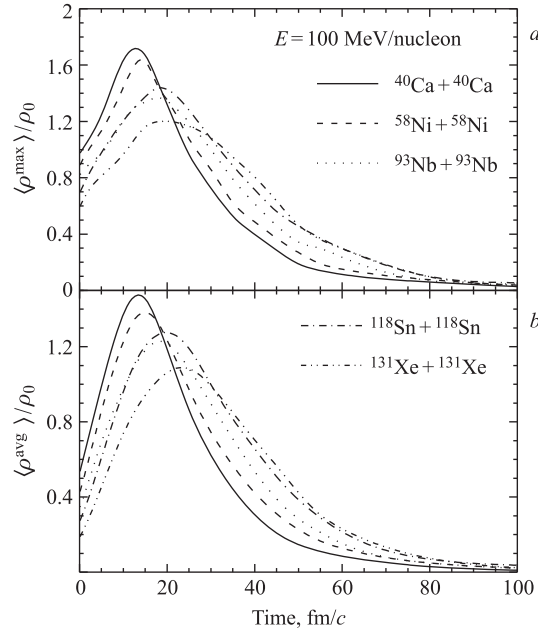


Fig. 1. The evolution of the maximum density $\langle \rho^{\text{max}} \rangle$ (a) and average density $\langle \rho^{\text{avg}} \rangle$ (b) reached in a central sphere of radius 2 fm as a function of time

In Fig. 1, *a* and *b*, we display the $\langle \rho^{\max} \rangle / \rho_0$ and $\langle \rho^{\text{avg}} \rangle / \rho_0$ as a function of reaction time. The displayed reactions are for the reactions of $^{40}\text{Ca} + ^{40}\text{Ca}$, $^{58}\text{Ni} + ^{58}\text{Ni}$, $^{93}\text{Nb} + ^{93}\text{Nb}$, $^{118}\text{Sn} + ^{118}\text{Sn}$ and $^{131}\text{Xe} + ^{131}\text{Xe}$ spreading over the whole mass range. It is evident that maximal ρ^{\max} for lighter systems is slightly higher compared to heavier ones. A similar trend can be seen for the evolution of ρ^{avg} . Also, in the lighter nuclei, reaction finishes much earlier compared to the heavier ones ($^{131}\text{Xe} + ^{131}\text{Xe}$). Similarly, the peaks in (the ρ^{\max} and ρ^{avg}) densities are also delayed in heavier nuclei compared to lighter ones. This is because the value of GVF is larger for heavier nuclei (0.8 for $^{131}\text{Xe} + ^{131}\text{Xe}$) compared to lighter nuclei (0.5 for $^{40}\text{Ca} + ^{40}\text{Ca}$). Due to the large value of GVF, the nucleon–nucleon collisions would be lesser and, therefore, less compression is achieved in these reactions. A wider density zone in heavier colliding nuclei over a long time span indicates the ongoing interactions among the nucleons, which is in agreement with the results as reported in [12].

Another quantity linked directly with the density is the collision rate. In Fig. 2, we display the net collision rate as a function of reaction time. Due to the larger interaction volume in heavier nuclei, the interactions among nucleons continue for a longer time, which is also evident from the density profile (Fig. 1). Further, a finite extended density zone in heavier nuclei leads to more nucleon–nucleon collisions. From the figure, we also see that the collision rate profile of Sn + Sn reaction is more extended compared to Nb + Nb. This behavior is opposite to what we have observed for other reaction from Ca + Ca to Nb + Nb. This is because the GVF is the same for Nb + Nb and Sn + Sn; therefore, there will be more binary collisions in Sn + Sn (because of greater mass) compared to Nb + Nb. On the other hand, the collision rate decreases as we move from Ca + Ca to Nb + Nb and from Sn + Sn

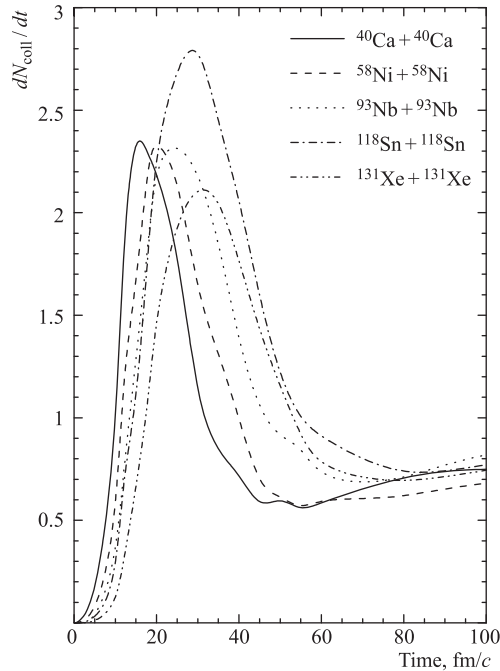


Fig. 2. Same as Fig. 1, but rate of allowed collisions dN_{coll}/dt versus reaction time

to Xe + Xe. This is because the GVF moves towards the peripheral geometries; therefore, there are less binary collisions even though the mass is increasing as we are moving towards peripheral geometries. Similar behavior can be noted from density profile also (compare dotted and dash-dotted lines).

It is well known from earlier studies [13] that participant-spectator matter acts as an indicator of the thermalization in a reaction. In the present study, we define the participant and spectator matter as: all the nucleons having experienced at least one collision are counted as *participant* matter. The remaining matter is labelled as *spectator* matter. The participant-spectator matter is scaled to the total mass of the reacting nuclei. These definitions give us the possibility of analyzing the reaction in terms of the participant-spectator fireball model. These definitions, however, are made of theoretical interest since the matter defined in these zones cannot be measured.

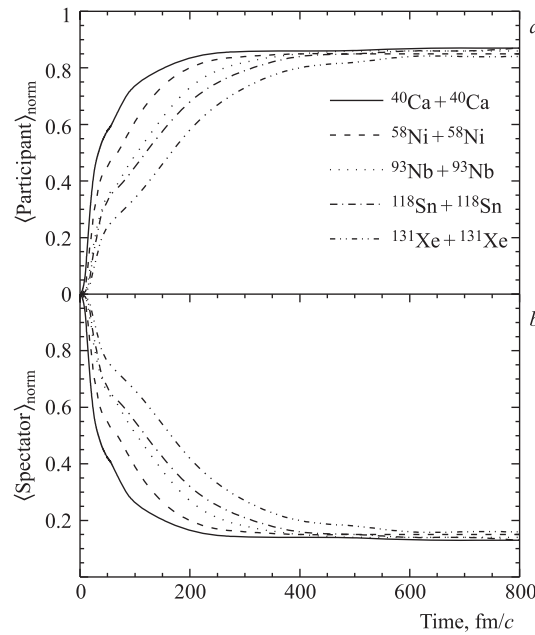


Fig. 3. The time evolution of normalized participant matter (a) and spectator matter (b) defined in terms of nucleon–nucleon collisions

In Fig. 3, we display the normalized participant matter (plot a) and spectator matter (plot b) as a function of reaction time. Here participant matter is defined using the nucleonic concept. As expected, at the start of the reaction, all the nucleons constitute spectator matter. Therefore, no participant matter exists at $t = 0$ fm/c. As the reaction proceeds, participant matter increases with the corresponding decrease of spectator matter. Since, for the case of lighter ones, reaction finishes much earlier, the transition from the spectator to participant matter is swift and sudden. On the other hand, in heavier colliding nuclei, the transition from spectator to participant is slow and gradual.

In Fig. 4, we display the maximal value of average and maximum density, labeled as $\langle \rho^{\text{avg}} \rangle$ and $\langle \rho^{\text{max}} \rangle$, respectively, versus composite mass of the system. Interestingly, the maximal

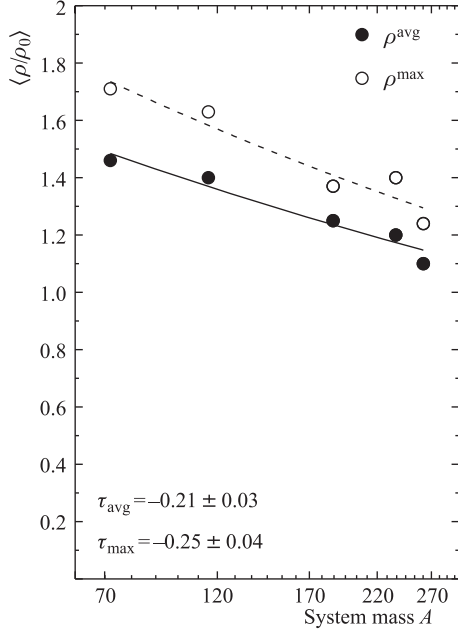


Fig. 4. The maximal value of $\langle \rho^{\text{max}} \rangle$ (open circles) and $\langle \rho^{\text{avg}} \rangle$ (closed circles) as a function of composite mass of the system. Lines represent a power law fit (αA^τ)

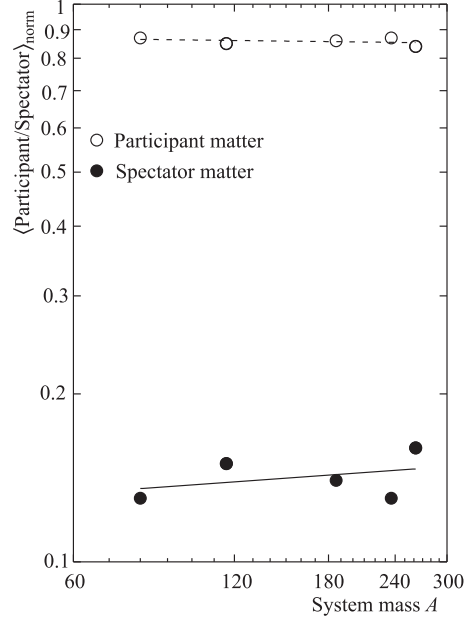


Fig. 5. The system size dependence of participant matter (open circles) and spectator matter (closed circles)

value of $\langle \rho^{\text{avg}} \rangle$ and $\langle \rho^{\text{max}} \rangle$ follows a power law (αA^τ) with τ being -0.21 ± 0.03 for the average density $\langle \rho^{\text{avg}} \rangle$ and -0.25 ± 0.04 for the maximum density $\langle \rho^{\text{max}} \rangle$. In other words, a slight decrease in the density occurs with increasing size of the system, as explained earlier.

The mass dependence of the participant and spectator matter is depicted in Fig. 5. From the figure, we see a nearly mass-independent behavior of participant and spectator matter. This is because the GVF is more (peripheral collisions) for heavier systems and is less for lighter systems. This means that in case of lighter systems, collisions are central and this counterbalances the mass effect (which otherwise will lead to decrease in participant matter in lighter systems, if the reactions are simulated at fix impact parameter).

The temperature during the simulations of heavy-ion collisions is calculated using Thomas–Fermi formalism. So, we first give the details of hot Thomas–Fermi formalism.

2.1. The Hot Thomas–Fermi Formalism. In a hot nuclear matter at temperature T , the momentum distribution of nucleons is given by Fermi–Dirac distribution

$$n(\mathbf{k}, T) = \frac{1}{1 + \exp\{[\tilde{\epsilon}(\mathbf{k}) - \mu]/T\}}. \quad (8)$$

Here $\tilde{\epsilon}(\mathbf{k})$ is the energy of the nucleon with momentum \mathbf{k} and μ is the chemical potential, which is determined by the normalization to a given density of nuclear matter ρ

$$\rho = \frac{g}{(2\pi)^3} \int_F n(\mathbf{k}) d\mathbf{k}, \quad (9)$$

where $g(= 4)$ is the spin-isospin degeneracy of a nucleon with momentum \mathbf{k} . The kinetic energy density ($\hbar^2\tilde{\tau}/2m$) and the entropy $\tilde{\sigma}$ are defined as

$$\tilde{\tau} = \frac{g}{(2\pi)^3} \int_F \mathbf{k}^2 n(\mathbf{k}) d\mathbf{k}, \quad (10)$$

$$\tilde{\sigma} = -\frac{g}{(2\pi)^3} \int_F \{n(\mathbf{k}) \ln n(\mathbf{k}) + [1 - n(\mathbf{k})] \ln [1 - n(\mathbf{k})]\} d\mathbf{k}. \quad (11)$$

All the integrations in the above equations (8)–(10) are performed over the whole Fermi sea F occupied by the hot nuclear matter. In a single nuclear matter limit, F is a diffuse Fermi sphere with its edge smeared out to infinity due to the finite temperature. When one uses the effective mass approximation for the single particle energies $\tilde{\epsilon}(\mathbf{k})$, i.e.,

$$\tilde{\epsilon}(\mathbf{k}) = \frac{\hbar^2 k^2}{2m} + U(\mathbf{k}) \simeq \frac{\hbar^2 k^2}{2m^*} + U(0), \quad (12)$$

Eq. (7) reads

$$n(\mathbf{k}, T) = \left\{ 1 + \exp \left[\frac{\hbar^2 k^2}{2m^* T} - \tilde{\eta} \right] \right\}^{-1}, \quad (13)$$

with $\tilde{\eta} = (\mu - U(0))/T$. In the single nuclear matter limit, the integration in Eqs. (8)–(10) can be performed in a standard way. For details, see [14].

But the momentum distribution of nucleons in the overlap region during a heavy-ion collision is not like that of single nuclear matter. F now consists of two Fermi spheres (say F_1 and F_2) separated by the relative momentum k_R (see Fig. 6). At the initial stages of the collision, k_R is large and is given by $\sqrt{2mE_{\text{lab}}}/\hbar^2$, with E_{lab} the incident energy per nucleon in the laboratory frame. As the collision proceeds, the target and projectile start to overlap and during the reaction, the area in momentum space between the two original Fermi spheres will be occupied and relative momentum starts becoming smaller and smaller. But even at the decomposition stage of the reaction, the average k_R still differs significantly

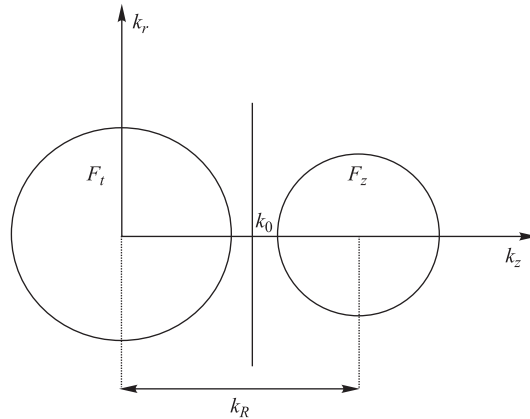


Fig. 6. Momentum distribution of nucleons in two colliding Fermi spheres separated by their relative momentum k_R . Here k_r and k_z are cylindrical coordinates

from zero. Therefore, it is necessary to take into account properly the deformed momentum distribution consisting of two interpenetrating Fermi spheres at each time step. In the study of the heavy-ion optical potentials at finite temperatures [15], the momentum distribution of the nucleons in two colliding nuclear matters at temperature T is evaluated in the rest frame of the nuclear matter with the higher density (say, F_1 in Fig. 6) and in cylindrical coordinates k_r, k_z , it can be written as

$$\begin{aligned} n(\mathbf{k}) = n_1(k_r, k_z) &= \frac{1}{1 + \exp[\hbar^2(k_r^2 + k_z^2)/(2m^*T) - \eta_1]} \quad \text{if } k_z < k_0, \\ n_2(k_r, k_z) &= \frac{1}{1 + \exp[\hbar^2(k_r^2 + (k_z - k_R)^2)/(2m^*T) - \eta_2]} \quad \text{if } k_z \geq k_0, \end{aligned} \quad (14)$$

with

$$k_0 = \frac{k_R^2 - 2m^*T(\tilde{\eta}_1 - \tilde{\eta}_2)}{2k_R}. \quad (15)$$

We note that k_0 is chosen in such a way that $n(\mathbf{k})$ is a continuous function of \mathbf{k} ; i.e., $n_1(k_r, k_0) = n_2(k_r, k_0)$ and $\tilde{\eta}_1$ and $\tilde{\eta}_2$ are determined by the normalization to the nuclear matter densities in the two Fermi spheres

$$\rho_i = \frac{g}{(2\pi)^3} \int_{V_i} n(\mathbf{k}) d\mathbf{k}, \quad (16)$$

where indices $i = 1, 2$ correspond to nucleons in the first (F_1) and second (F_2) Fermi spheres, respectively. V_1 and V_2 are the volumes in momentum space with $k_z < k_0$ and $k_z \geq k_0$, respectively. The kinetic energy density ($\hbar^2\tilde{\tau}/2m$) and the entropy $\tilde{\sigma}$ are defined in the same way as for the one-Fermi-sphere case:

$$\tilde{\tau}_i = \frac{g}{(2\pi)^3} \int_{V_i} \mathbf{k}^2 n(\mathbf{k}) d\mathbf{k}, \quad (17)$$

$$\tilde{\sigma}_i = -\frac{g}{(2\pi)^3} \int_{V_i} \{n(\mathbf{k}) \ln n(\mathbf{k}) + [1 - n(\mathbf{k})] \ln [1 - n(\mathbf{k})]\} d\mathbf{k}. \quad (18)$$

Here all integrations must be performed over the cylindrical coordinates k_r, k_z with the center chosen as that of the big sphere (F_1). For details, see [12]. In order to calculate the local temperature at each point \mathbf{r} in each time step, we need to know the matter density and the kinetic energy densities of the target and the projectile which are given as

$$\rho_T(\mathbf{r}, t) = \sum_{i=1}^{A_T} \rho_i(\mathbf{r}, t), \quad \rho_P(\mathbf{r}, t) = \sum_{i=1}^{A_P} \rho_i(\mathbf{r}, t) \quad (19)$$

and

$$\tilde{\tau}_T(\mathbf{r}, t) = \sum_{i=1}^{A_T} \frac{\mathbf{p}_i^2(t)}{2m} \rho_i(\mathbf{r}, t), \quad \tilde{\tau}_P(\mathbf{r}, t) = \sum_{i=1}^{A_P} \frac{\mathbf{p}_i^2(t)}{2m} \rho_i(\mathbf{r}, t), \quad (20)$$

where $\rho_i(\mathbf{r}, t)$ is given by Eq. (6).

Note that $\rho(\mathbf{r}, t) = \sum_{i=1}^{A_T+A_P} \rho_i(\mathbf{r}, t)$ gives us the total matter density in coordinate space.

These matter densities and kinetic energy densities are calculated in the simulation at the position of each particle in each time step. Using these four values, one can calculate by inversion the expressions of Eqs. (8), (9) and (11) $\tilde{\eta}_1$ and $\tilde{\eta}_2$ connected with the Fermi energies, the local temperature T and the relative momentum k_R . These equations are solved by transferring the coordinate space and the momentum space to the frame of the nucleus which has the higher density at the point (\mathbf{r}, t) considered. Since it is very time-consuming to solve these equations at each time step, we generate first 4-dimensional tables of $(\rho_1, \rho_2, \tilde{\tau}_1, \tilde{\tau}_2)$ as a function of $(\tilde{\eta}_1, \tilde{\eta}_2, T, k_R)$ for the values which can be extracted from the simulation of heavy-ion reactions within IQMD. At each time step during the evolution of the heavy-ion system, these tables are used to obtain $\tilde{\eta}_1, \tilde{\eta}_2$, and the temperature T by inverse interpolation from the actual values $\rho_1, \rho_2, \tilde{\tau}_1, \tilde{\tau}_2$ found in the simulation. It is worth mentioning that due to this complicated procedure of extraction of temperature at the position of individual nucleons in each time step, the calculation time increases drastically.

In principle, a true temperature can be defined only for a thermalized and equilibrated matter. Since in heavy-ion collisions the matter is non-equilibrated, one cannot talk of temperature. However, one can look in terms of the local environment only. In the present case, we follow the description of temperature as given in [12, 16]. The extraction of the temperature T is based on the local density approximation; that is, one deduces the temperature in a volume element surrounding the position of each particle at a given time step [12, 16]. Here, we postulate that each volume element of nuclear matter in coordinate space and time has some

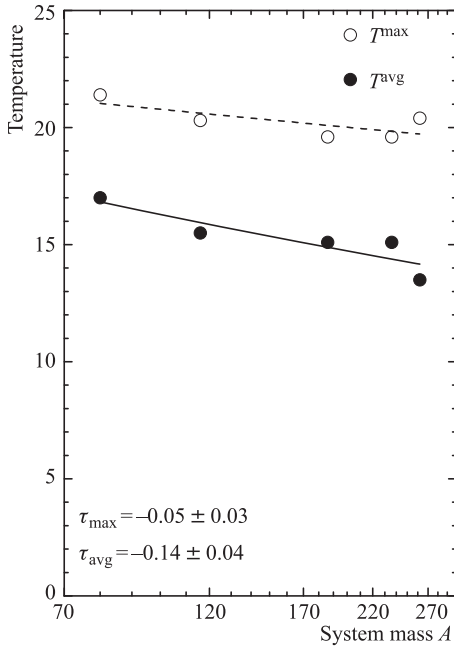


Fig. 7. Same as Fig. 5, but for the maximal value of the average temperature

«temperature» defined by the diffused edge of the deformed Fermi distribution consisting of two colliding Fermi spheres, which is typical for a nonequilibrium momentum distribution in heavy-ion collisions.

In this formalism (dubbed the hot Thomas–Fermi approach) [12], one determines extensive quantities such as the density and kinetic energy as well as entropy with the help of momentum distributions at a given temperature. The details of the formalism have been discussed earlier. Using this formalism, we also extracted the average and maximum temperature within a central sphere of 2-fm radius as described in the case of density.

In Fig. 7, we plot the maximal value of average and maximum temperature labeled as $\langle T^{\text{avg}} \rangle$ and $\langle T^{\text{max}} \rangle$, respectively, as a function of composite mass of the system. One sees that both these quantities can be parameterized in terms of power law function αA^τ , τ being equal to -0.14 ± 0.04 and -0.05 ± 0.03 , respectively, for the average and maximum temperature. Hence, one can conclude that both average and maximum temperatures show a little dependence on system

size. Since in our present case we have carried out the study at fixed incident energy, this leads to little dependence of temperature on the system mass.

3. SUMMARY

We have studied the mass dependence of various quantities (such as average and maximum central density, temperature and participant spectator matter) at the geometry of vanishing flow. Our calculations present several interesting facts. The reaction saturation time is smaller for lighter nuclei compared to heavier ones. The maximal value of the density, temperature and collision rate are also shifted accordingly. In all the cases, a power law dependence can be seen. All the quantities are found to be nearly mass-dependent except participant spectator matter, which is found to be mass-independent.

Acknowledgements. The author is grateful to Dr. Rajeev K. Puri, Department of Physics, Panjab University, Chandigarh, for his valuable discussions.

REFERENCES

1. *Scheid W., Muller H., Greiner W.* Nuclear Shock Waves in Heavy-Ion Collisions // *Phys. Rev. Lett.* 1974. V. 32. P. 741;
Gustafson H. A., Gustafson H. H., Kolb B. Collective Flow Observed in Relativistic Nuclear Collision // *Phys. Rev. Lett.* 1984. V. 52. P. 1590.
2. *Sood A. D., Puri R. K.* Nuclear Dynamics at the Balance Energy // *Phys. Rev. C.* 2004. V. 70. P. 034611; Mass Dependence of Disappearance of Transverse In-Plane Flow // *Ibid.* V. 69. P. 054612; Study of Balance Energy in Central Collisions for Heavier Nuclei // *Phys. Lett. B.* 2004. V. 594. P. 260; Influence of Momentum Dependent Interactions on Balance Energy and Mass Dependence // *Eur. Phys. J. A.* 2006. V. 30. P. 571;
Puri R. K., Kumar S. Binary Breakup: Onset of Multifragmentation and Vaporization in Ca–Ca Collision // *Phys. Rev. C.* 1998. V. 57. P. 2744;
Chugh R., Puri R. K. Importance of Momentum Dependent Interactions at the Energy of Vanishing Flow // *Phys. Rev. C.* 2010. V. 82. P. 014603.
3. *Gautam S. et al.* Isospin Effects on the Energy of Vanishing Flow in Heavy-Ion Collisions // *J. Phys. G: Nucl. Part. Phys.* 2010. V. 37. P. 085102; Sensitivity of Transverse Flow to the Symmetry Energy // *Phys. Rev. C.* 2011. V. 83. P. 034606; Isospin Effects in the Disappearance of Flow as a Function of Colliding Geometry // *Ibid.* P. 014603;
Kumar S. et al. Impact Parameter Dependence of the Disappearance of Flow and In-Medium Nucleon–Nucleon Cross Section // *Phys. Rev. C.* 1998. V. 58. P. 3494.
4. *Ogilvie C. A., Cebra D. A., Clayton J.* Transverse Collective Motion in Intermediate Energy Heavy-Ion Collisions // *Phys. Rev. C.* 1989. V. 40. P. 2592;
Blattel B., Koch V., Lang A. Origin of Transverse Momentum in Relativistic Heavy-Ion Collisions: Microscopic Study // *Phys. Rev. C.* 1991. V. 43. P. 2728;
Andronic A., Reisdorf W., Herrmann N. Directed Flow in Au + Au, Xe + CsI, Ni + Ni Collisions and Nuclear Equation of States // *Phys. Rev. C.* 2003. V. 67. P. 034907;
Goyal S., Puri R. K. On the Sensitivity of the Energy of Vanishing Flow towards Mass Asymmetry of Colliding Nuclei // *Nucl. Phys. A.* 2011. V. 853. P. 164.
5. *Krofcheck D., Bauer W., Crawley G. M.* Disappearance of Flow in Heavy-Ion Collisions // *Phys. Rev. Lett.* 1989. V. 63. P. 2028.

6. *Majestro D.J., Bauer W., Bjarki O.* Disappearance of Transverse Flow in Au + Au Collisions // *Phys. Rev. C.* 2000. V. 61. P. 021602(R);
Majestro D.J., Bauer W., Westfall G.D. Isolation of the Nuclear Compressibility with the Balance Energy // *Ibid.* V. 62. P. 041603(R).
7. *Chugh R. K., Sood A. D.* Geometry of Vanishing Flow: A New Probe to Determine the In-Medium Nucleon–Nucleon Cross Section // *Parmana J. Phys.* 2011. V. 77. P. 289.
8. *Puri R. K. et al.* Study of Non-Equilibrium Effects and Thermal Properties of Heavy-Ion Collisions Using a Covariant Approach // *J. Phys. G.* 1994. V. 20. P. 1817.
9. *Hartnack C., Puri R. K., Aichelin J.* Modelling the Many-Body Dynamics of Heavy-Ion Collisions: Present Status and Future Perspective // *Eur. Phys. J. A.* 1998. V. 1. P. 151;
Kumar S. et al. Effect of the Symmetry Energy on Nuclear Stopping and Its Relation to the Production of Light Charged Fragments // *Phys. Rev. C.* 2010. V. 81. P. 014601; Elliptical Flow and Isospin Effects in Heavy-Ion Collisions at Intermediate Energies // *Ibid.* P. 014611;
Kaur V. et al. On Elliptical Flow and Mass Asymmetry of the Colliding Nuclei // *Phys. Rev. B.* 2011. V. 697. P. 512; On Nuclear Stopping in Asymmetric Colliding Nuclei // *Nucl. Phys. A.* 2011. V. 861. P. 37.
10. *Khoa D. T. et al.* In-Medium Effects in the Description of Heavy-Ion Collisions with Realistic Nucleon–Nucleon Interactions // *Nucl. Phys. A.* 1992. V. 548. P. 102;
Lehmann E. et al. Study of In-Medium Effects on the Disappearance of the Sideways Flow in Heavy-Ion Collisions // *Z. Phys. A.* 1996. V. 355. P. 55;
Sood A. D., Puri R. K. Nuclear Dynamics at the Balance Energy // *Phys. Rev. C.* 2004. V. 70. P. 034611.
11. *Kaur M., Gautam S.* On the Isospin Effects in the Geometry of Vanishing Flow in Heavy-Ion Collisions // *Phys. Part. Nucl. Lett.* 2013. V. 10, No. 3. P. 228–233.
12. *Khoa D. T., Ohtsuka N., Faessler A.* Microscopic Study of Thermal Properties of the Nuclear Matter Formed in Heavy-Ion Collisions // *Nucl. Phys. A.* 1992. V. 542. P. 671.
13. *Sood A. D., Puri R. K.* Participant Spectator Matter at the Energy of Vanishing Flow // *Phys. Rev. C.* 2000. V. 79. P. 064618; Study of Participant-Spectator Matter and Collision Dynamics in Heavy-Ion Collision // *Intern. J. Mod. Phys. E.* 2006. V. 15. P. 899;
Gautam S. Participant-Spectator Matter and Thermalization of Neutron-Rich Systems at the Energy of Vanishing Flow // *Phys. Rev. C.* 2012. V. 85. P. 067601.
14. *Barranco M., Treiner J.* Self-Consistent Description of Nuclear Level Densities // *Nucl. Phys. A.* 1981. V. 351. P. 269.
15. *Rashdan M. et al.* The Temperature Dependence of the Hi Optical Potential // *Nucl. Phys. A.* 1987. V. 468. P. 168.
16. *Khoa D. T., Ohtsuka N., Matin M. A.* In-Medium Effects in Description of Heavy-Ion Collisions with Realistic Nucleon–Nucleon Interactions // *Nucl. Phys. A.* 1992. V. 548. P. 102;
Puri R. K., Ohtsuka N., Lehmann E. Temperature-Dependent Mean Field and Its Effect on Heavy-Ion Reactions // *Nucl. Phys. A.* 1994. V. 575. P. 733.

Received on September 1, 2012.